# Self-similar spectral structures and edge-locking hierarchy in open-boundary spin chains

Masudul Haque
*Max-Planck Institute for the Physics of Complex Systems, Nöthnitzer Strasse 38, D-01187 Dresden, Germany*
(Received 14 April 2010; published 22 July 2010)

For an anisotropic Heisenberg (*XXZ*) spin chain, we show that an open boundary induces a series of approximately self-similar features at different energy scales, high up in the eigenvalue spectrum. We present a nonequilibrium phenomenon related to this fractal structure, involving states in which a connected block near the edge is polarized oppositely to the rest of the chain. We show that such oppositely polarized blocks can be "locked" to the edge of the spin chain and that there is a hierarchy of edge-locking effects at various orders of the anisotropy. The phenomenon enables dramatic control of quantum-state transmission and magnetization control.

DOI: 10.1103/PhysRevA.82.012108 PACS number(s): 03.65.Ge, 75.10.Pq, 03.65.Xp, 03.67.Ac

## I. INTRODUCTION

Rapid advances in nanostructure and cold-atom technologies have ensured that explicit temporal evolution of many-body quantum states far from equilibrium are no longer of academic interest only, as was the case in the traditional bulk solid-state context. In such novel nonequlibrium settings, spectral features far from the ground state can be as important as the properties of low-lying excitations. Partly motivated by these new possibilities, there has been intense theoretical interest in the control of quantum states, for example, quantum-state transfer through spin chains [1].

In this work, we present and analyze a phenomenon associated with the high-energy spectrum of open-boundary spin-$\frac{1}{2}$ chains governed by an anisotropic Heisenberg interaction, that is, open *XXZ* chains. The open boundary causes a hierarchy of self-similar structures at different energy scales. This "fractal" structure is not present in the periodic spin chain but pops into existence when a single bond is severed to produce an open chain. We demonstrate an associated dynamical effect—a block of spins anti-aligned to an otherwise polarized background can be spatially "locked" if placed appropriately at or near the edge. We reveal the sense in which these configurations are close to being stationary states of the Hamiltonian. The presence of such stable arrangements open up simple but powerful possibilities for controlling spin state (magnetization) transport through operations on a few spins.

The *XXZ* chain is a basic model of condensed-matter physics and has long been the subject of sustained theoretical activity. The open chain has received far less detailed attention than the periodic case, and even less material is available for physics far from the ground state. Localization phenomena and intricate spectral structures in the *XXZ* chain are thus obviously of fundamental interest. In addition, the *XXZ* model has recently been shown to describe Josephson junction arrays of the flux qubit type [2] and also may be realizable in optical lattices [3] or with polaritons in coupled arrays of cavities [4]. The mechanisms for quantum control uncovered by our results should be possible to implement in one of these setups in the foreseeable future.

The open antiferromagnetic *XXZ* chain with $L$ sites is described by the Hamiltonian

$$H_{XXZ} = J_x \sum_{j=1}^{L-1} \left( S_j^x S_{j+1}^x + S_j^y S_{j+1}^y + \Delta S_j^z S_{j+1}^z \right).$$

The $S^z S^z$ term acts as an "interaction," penalizing alignment of neighboring spins. The in-plane terms $(S_j^x S_{j+1}^x + S_j^y S_{j+1}^y) = \frac{1}{2}(S_j^+ S_{j+1}^- + S_j^- S_{j+1}^+)$ provide "hopping" processes. Since $H_{XXZ}$ preserves total $S^z$, the dynamics is always confined to sectors of fixed numbers $N_\uparrow$ of up-spins. We mostly consider the large $\Delta$ regime, where the localization phenomena to be described are most robust. Energy and time are measured in $J_z = J_x\Delta$ and $J_z^{-1} = (J_x\Delta)^{-1}$ units. Hopping is an $O(\Delta^{-1})$ process in these units.

We first describe in Sec. II the dynamical phenomenon, namely, the hierarchy of edge-locked configurations. In Sec. III, we describe the effect of the open boundary on the spectrum, in particular the self-similar structure and how this structure explains the edge-locking effects. Section IV explains how the hierarchy of spectral separations can be understood from the competition between two mechanisms in degenerate perturbation theory. Section V points out possibilities for using the edge-locking phenomena as the basis for control mechanisms of magnetization transport.

## II. EDGE-LOCKED STATES

In Fig. 1, we show some example configurations, that is, positions of up-spin blocks near the edge in a background of down-spins. In the configurations shown on the left, the $\uparrow$ blocks are locked by the edge at large $\Delta$, while the $\uparrow$'s in the right-column configurations are not edge locked. In dynamic terms, the configurations in the left column are *stable*, while those shown on the right decay away. Of course, stability should be understood in terms of time scales relevant to the edge-locking physics and are not absolute.

The simplest and most robust edge states are those in which the block starts at the very edge site, such as configurations a through d in Fig. 1. Even a single $\uparrow$ spin placed in this way is localized at the edge. For $N_\uparrow$ up-spins placed this way, we call these configurations $|L_{N_\uparrow,(1)}\rangle$ or $|R_{N_\uparrow,(1)}\rangle$, depending on whether the block is at the left edge or right edge of the chain. Figs. 1(a) through 1(d) are thus $|L_{1,(1)}\rangle$ through $|L_{4,(1)}\rangle$. The subscript (1) indicates that the $\uparrow$ blocks start at site $j = 1$.

The second class of edge states are those where the block starts at the $j = 2$ site (or ends at $j = L - 1$). We call these $|L_{N_\uparrow,(2)}\rangle$ or $|R_{N_\uparrow,(2)}\rangle$. For such states to be edge locked, one needs blocks of three or more $\uparrow$'s, that is, $N_\uparrow \geqslant 3$. This is indicated in Fig. 1 by showing $|L_{1,(2)}\rangle$, $|L_{2,(2)}\rangle$ on the

 

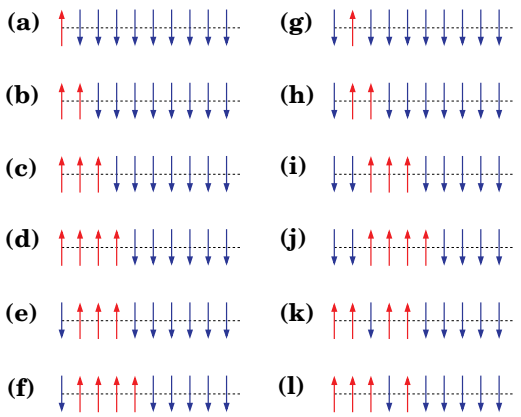


FIG. 1. (Color online) A few ↑ spins at the left edge of an almost polarized spin chain. The leftmost ten spins are shown; the remaining spins to the right are all ↓'s. The configurations on the left (a–f) are edge locked, while those on the right (g–l) are not.

right column (not edge locked) as g and h, and $|L_{3,(2)}\rangle$, $|L_{4,(2)}\rangle$ on the left column (edge locked) as e and f. Similarly, blocks starting at $j = 3$ (or ending at $j = L - 2$) are stable only for $N_\uparrow \geqslant 5$. Generalizing, state $|L_{N_\uparrow,(k)}\rangle$ having a block starting at site $k$ will be stable via edge-locking only if $N_\uparrow \geqslant (2k - 1)$.

The edge-locking effects are due to spectral separation of the stable states from other states (Sec. III), which prevents hybridizations that might enable propagation of the oppositely polarized blocks. The spectral separation can be understood using perturbative arguments at small $\Delta^{-1}$. In the hierarchy described previously, the first class of edge locking (blocks starting at the edge site) is a zeroth-order effect, while edge locking at the second level (blocks starting at next-to-edge site) is an $O(\Delta^{-2})$ effect. Generally, the level-$k$ edge locking of this hierarchy is an $O(\Delta^{-2(k-1)})$ effect.

### A. Temporal dynamics

Figure 2 demonstrates the edge-locking phenomenon through explicit time evolution of several configurations. The top row shows the evolution of $N_\uparrow = 2$ states $|L_{2,(1)}\rangle$ and $|L_{2,(2)}\rangle$. The first is an edge-locked state and shows very little evolution, while the second is not locked, and thus the ↑↑ block propagates to the right.

The lower panels show $N_\uparrow = 3$ states. Now there are two configurations where the ↑↑↑ block is locked by the left edge. We have chosen a moderate value of $\Delta$ so that the $O(\Delta^{-2})$ locked state $|L_{3,(2)}\rangle$ can be clearly seen to have weaker locking than the $O(\Delta^0)$ locked state $|L_{3,(1)}\rangle$. [Figure 2(d) has more dynamics and larger oscillations than 2(c).] Obviously, the higher order locking can be made more robust by using a larger $\Delta$.

Figure 2 shows results for $L = 18$ sites, but a longer chain displays identical time evolutions at the time scales shown. The size plays a role only when the propagating block meets the other edge and gets reflected. It is clear that the unlocked blocks in Figs. 2(b) and 2(e) are still propagating to the right at the time scales shown.

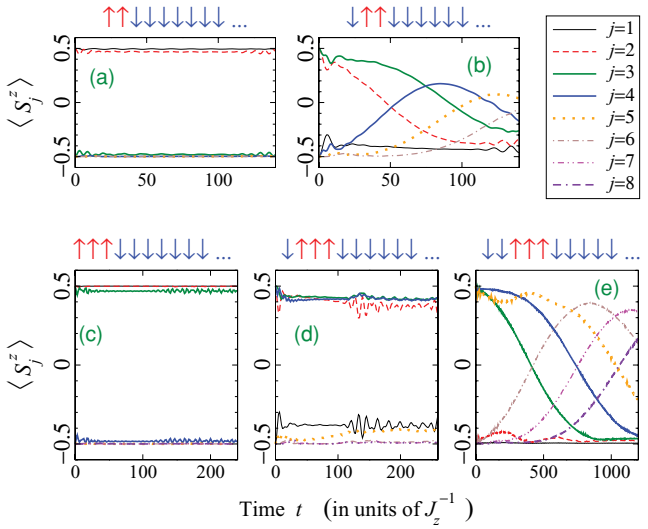


FIG. 2. (Color online) Dynamics of open $XXZ$ chain ($\Delta = 4$), initiated with $N_\uparrow = 2$ or $N_\uparrow = 3$ oppositely polarized spins near the left edge. Initial configurations are shown on top of each panel. In the edge-locked cases (a, c, d), local spin values $\langle S_j^z \rangle$ do not vary much from their initial values.

## III. SPECTRAL STRUCTURES

The hierarchy of edge-locking effects presented in Sec. II is intimately related to (and is due to) intricate structures in the eigenvalue spectrum of the open $XXZ$ chain. In this section, we describe the hierarchy of spectral separations and explain how these structures lead to the edge-locking hierarchy.

### A. Periodic versus open chain

Figure 3 shows energy spectra in the $N_\uparrow = 3$ sector. At large $\Delta$, the spectrum separates into well-separated bands. In the periodic chain, the bands correspond to cases where the three ↑ spins are next to each other (top band), two are next to each other (middle band), or no two ↑ spins neighbor each other (bottom band). In general, with $N_\uparrow$ ($< L/2$) up-spins in a periodic large-$\Delta$ chain, the spectrum is separated into $N_\uparrow$ bands. The topmost band is maximally ferromagnetic and has the minimal number (two) of favorable ↑-↓ bonds and $(L - 2)$ unfavorable (↑-↑ or ↓-↓) bonds.

Figure 3(b) shows the effect of open boundaries. The spectrum described previously for the periodic chain now acquires an explosion of additional features. The periodic-chain bands get split, because the edge allows additional possibilities for numbers of favorable and unfavorable bonds. In addition, several of these new bands have additional substructures. While these structures are all interesting and deserve to be analyzed in detail, in this work we are only be concerned with the top two bands of the open chain, which both emerge from the topmost band of the periodic chain and hence are related to periodic-chain configurations with all ↑ spins in a connected block.

### B. Spectral explanation of edge locking

The topmost band has only two states, and these are the most obvious edge-locked states. At $\Delta^{-1} = 0$, this is a degenerate

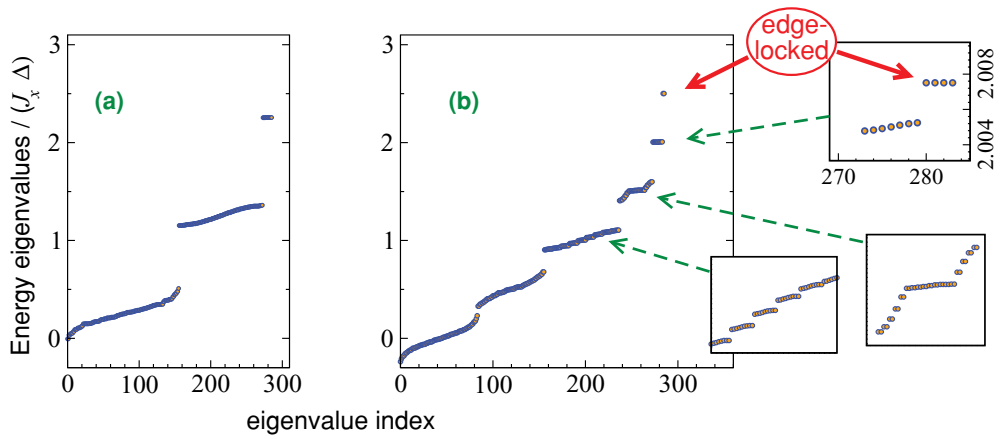


FIG. 3. (Color online) Energy spectra for (a) periodic *XXZ* chain and (b) open *XXZ* chain. In each case, $L = 13$, $N_\uparrow = 3$, and $\Delta = 10$. Compared to the periodic chain, the open-chain spectrum has extra features, some of which are highlighted in insets. With $N_\uparrow = 3$, there are two classes of edge-locked states, the two states of the top band (main plot) and two of the four states separating out from the next band (upper inset). The lower insets show additional spectral structures induced by the edge.

two-dimensional manifold spanned by $|L_{N_\uparrow,(1)}\rangle$ and $|R_{N_\uparrow,(1)}\rangle$. At finite $\Delta^{-1}$, other configurations contribute to the two states, but for small enough $\Delta^{-1}$, the eigenstates are dominated by $|L_{N_\uparrow,(1)}\rangle \pm |R_{N_\uparrow,(1)}\rangle$.

The edge block in $|L_{N_\uparrow,(1)}\rangle$ is strongly locked because this state is hybridized mainly with $|R_{N_\uparrow,(1)}\rangle$. From $|L_{N_\uparrow,(1)}\rangle$, it is energetically possible to tunnel into the $|R_{N_\uparrow,(1)}\rangle$ state, but such a process is exponentially suppressed at large chain lengths. Thus $|L_{N_\uparrow,(1)}\rangle$ can be regarded as stationary for practical purposes, as Figs. 2(a) and 2(c) demonstrate dynamically.

The other edge-locking effects are weaker and can be seen by zooming into the second band from the top, which consists of configurations with two favorable bonds [Fig. 3(b), upper inset]. Four states separate out from the rest of this band, with $O(\Delta^{-2})$ splitting. For $N_\uparrow = 3$, these four states are linear combinations of $|L_{3,(2)}\rangle$, $|R_{3,(2)}\rangle$, and

$$|\uparrow\uparrow\downarrow\downarrow\downarrow \ldots \downarrow\downarrow\downarrow\uparrow\rangle \quad \text{and} \quad |\uparrow\downarrow\downarrow\downarrow \ldots \downarrow\downarrow\downarrow\uparrow\uparrow\rangle.$$

The rest of the band is dominated by linear combinations of the remaining configurations containing the ↑ spins in connected blocks farther from the edge.

Due to the spectral separation, the four states are not hybridized with the remaining block configurations. This locks the $|L_{3,(2)}\rangle$ and $|R_{3,(2)}\rangle$ configurations to their respective edges, because from any of these states, tunneling to the other three of the submanifold is a very high-order process.

### C. Fractal hierarchy in spectrum

For $N_\uparrow = 3$, only the first two classes of edge-locked states are present, as indicated by the two solid arrows in Fig. 3(b). An additional level of the hierarchy becomes available with each increase of $N_\uparrow$ by two. The associated spectral separations can be seen by successively zooming in within the next-to-top band. Figure 4 (left four panels) shows this for $N_\uparrow = 8$, where four edge-locked configurations appear. Figure 4 (right) displays the associated gaps scaling as $\delta_k \sim \Delta^{2k-1}$.

For large $N_\uparrow$ and long chains ($L > 2N_\uparrow$), the same structure of four states separating from the rest can be seen at many different energy scales by successively zooming in, and the successive structures become more self-similar, that is, a fractal structure emerges in the large-$N_\uparrow$, large-$L$, limit.

## IV. PHYSICAL REASON FOR SPECTRAL SEPARATIONS

The spectral separation of the top two states is relatively trivial: $|L_{N_\uparrow,(1)}\rangle$ and $|R_{N_\uparrow,(1)}\rangle$ are the only configurations having a *single* favorable anti-aligned bond and therefore have higher energy than the next $(L-2)$ states which involve configurations with two favorable bonds.

The higher levels of the spectral-separation hierarchy are more subtle and can be understood through power counting based on degenerate perturbation theory around the Ising ($\Delta^{-1} = 0$) limit. We give a brief explanation for the second level, namely the separation of states $|L_{N_\uparrow,(2)}\rangle$ and $|R_{N_\uparrow,(2)}\rangle$ from the states $|L_{N_\uparrow,(k)}\rangle$ with $2 < k < (L - N_\uparrow)$.

At $\Delta^{-1} = 0$, the configurations with two favorable bonds are all degenerate. At small finite $\Delta^{-1}$, these spread out to form the next-to-top band. The hybridization of these levels

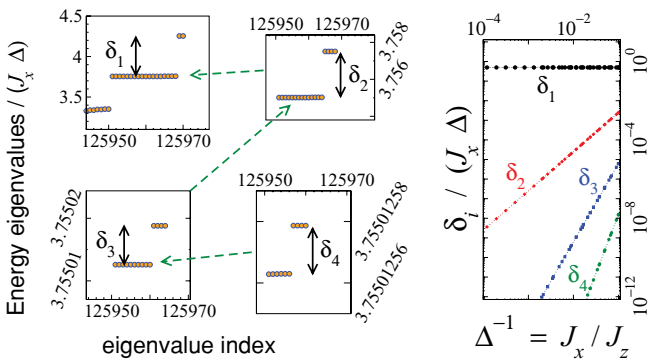


FIG. 4. (Color online) Left: hierarchy of subband splittings seen by zooming in successively. Here $N_\uparrow = 8$ ($L = 20$, $\Delta = 10$), so the first four levels of the hierarchy are present. For large $N_\uparrow$ and $L$, the splitting structures are self-similar. Right: Energy splittings scale as $\delta_1 \sim \Delta^0$, $\delta_2 \sim \Delta^{-2}$, $\delta_3 \sim \Delta^{-4}$, and $\delta_4 \sim \Delta^{-6}$.

happens at order $\Delta^{-N_\uparrow}$, because $N_\uparrow$ hops are required to connect configurations $|L_{N_\uparrow,(k)}\rangle$ and $|L_{N_\uparrow,(k+1)}\rangle$, for example,

$$|L_{3,(k)}\rangle = (S^+_{k+2}S^-_{k+3})(S^+_{k+1}S^-_{k+2})(S^+_k S^-_{k+1})|L_{3,(k+1)}\rangle$$

for $N_\uparrow = 3$. Thus, the spreading or dispersion of the next-to-top band is of order $\Delta^{-N_\uparrow}$.

On the other hand, since each $|L_{N_\uparrow,(k)}\rangle$ is connected to itself by two hops, for example,

$$|L_{N_\uparrow,(k)}\rangle = (S^+_k S^-_{k-1})(S^+_{k-1}S^-_k)|L_{N_\uparrow,(k)}\rangle,$$

the states acquire energy shifts at order $\Delta^{-2}$. Considering the energies of the intermediate states in this process, one can see that the states $|L_{N_\uparrow,(2)}\rangle$ and $|R_{N_\uparrow,(2)}\rangle$ have a different energy shift compared to the rest, due to the edge. For example, the intermediate state in this process for $|L_{3,(2)}\rangle$ is $|\uparrow\downarrow\uparrow\uparrow\downarrow\downarrow\downarrow\ldots\rangle$, which has an $\uparrow$ at the edge, while the intermediate state in the case of $|L_{3,(k>2)}\rangle$ is of type $|\downarrow\ldots\downarrow\uparrow\downarrow\uparrow\uparrow\downarrow\downarrow\downarrow\ldots\rangle$, where the lone $\uparrow$ is in the interior. The intermediate states have energies differing by $\sim\Delta/2$ due to differing numbers of favorable bonds. This leads to different $O(\Delta^{-2})$ shifts for $|L_{3,(2)}\rangle$ compared to that for $|L_{3,(k>2)}\rangle$.

This $O(\Delta^{-2})$ separating effect competes with the $O(\Delta^{-N_\uparrow})$ hybridization. The separating effect wins only for $N_\uparrow > 2$, which is why the second level of the spectral gap hierarchy exists only for $N_\uparrow > 2$.

The argument is readily extended to higher stages of the hierarchy. Blocks starting at site $k$ have an $O(\Delta^{-2(k-1)})$ shift distinct from the shift of the farther blocks and hence will be separated from the band if $2(k-1) < N_\uparrow$.

## V. QUANTUM CONTROL PROTOCOLS

The edge-locking phenomenon provides many opportunities for controlling the evolution and transport of magnetization, provided that the experimental realization of the *XXZ* chain allows single-site (or few-site) addressing. We point out the most obvious possibilities.

If single-site spin-flipping probes ($\pi$ pulse) can be implemented, this can be used as a quantum switch to release a locked block. For example, by flipping the first spin of the locked block in $|L_{3,(1)}\rangle$, one gets the state $|L_{2,(2)}\rangle$, in which the two-site block is not locked [Fig. 2(h)] and so starts propagating. Similarly, by starting with a five- or six-site oppositely polarized block at the edge, applying a $\pi$ pulse on the first *two* sites initiates the transmission of a signal consisting of a block of spins anti-aligned to the background. Once the signal reaches the other edge, the block could also be locked to the other edge by $\pi$ pulsing one or two spins at the other edge at the appropriate time.

More complex dynamics can be launched by applying a $\pi$ pulse to a site internal to the locked block, for example, by flipping the second site of the locked $|L_{4,(1)}\rangle$ configuration. The resulting state $\uparrow\downarrow\uparrow\uparrow\downarrow\downarrow\downarrow\downarrow\ldots$ has the following dynamics: the $\uparrow$ at site 3 moves to site 2 so that a two-site $\uparrow\uparrow$ block then stays locked to the edge, while a third $\uparrow$ propagates to the right. While a complete explanation involves the lower energy bands, which are beyond the scope of this article, the tendency to lock blocks at the edge is clearly seen here too.

It is remarkable that these control mechanisms for magnetization transport do not require fine-tuned or spatially varying interactions, as is common in the quantum-state transfer literature [1]. The relevant physics here arise simply due to an open edge.

## VI. DISCUSSION

In this work, we have presented a hierarchy of self-similar spectral separations in the open *XXZ* chain with large Ising anisotropy. Associated with these spectral structures is a hierarchy of edge-locking effects, which can be exploited for the control of magnetization transport if single-site addressing can be implemented in an *XXZ* chain realization.

### A. Comments on the self-similar structures

In general, one can expect that at large $\Delta$ each eigenenergy can be expanded separately in $\Delta^{-1}$, so that structures at every scale (every order in $\Delta^{-1}$) might be expected to be generic. However, as we have seen, in periodic chains the contributions at every higher order tend to be the same for each eigenstate within a band, so no structures appear. The presence of an edge creates an opportunity to have different contributions for different eigenstates, leading to subband structures at many different scales.

We have used the word "fractal" in the colloquial sense, where the word describes any self-similar structure. A more rigorous usage would involve consideration of the fractal dimension of the set under consideration. Unfortunately, for discrete sets, fractal dimensions are often ambiguous and can have different values for different definitions. In our case, the set under question has points separated by distances of order $1, x, x^2, x^3, \ldots$ $(x = \Delta^{-2})$. The box-counting dimension (Minkowski-Bouligand dimension) is zero for this set, but it is not ruled out that another common definition of fractal dimension could give a nonzero value.

### B. Itinerant models

Edge-related localization and spectral separation were reported previously in itinerant models [5,6]. The physics in Refs. [5,6] correspond to only the second level of the hierarchy reported here. The first level is absent in those itinerant models. To the best of our knowledge, the existence of an entire fractal structure and the associated dynamical hierarchy, arising from severing a single bond of the periodic chain, has never been noted. A similar hierarchy presumably exists also in the itinerant models but has yet to be studied.

The *XXZ* chain model is generally considered to be equivalent to the spinless fermion model with nearest-neighbor couplings. However, if the interaction is of $Vn_in_{i+1}$ form as in Ref. [6] ($n_i$ are site occupancies), the spectral structure associated with open-chain edge localization is strikingly different from the *XXZ* chain. The physics becomes identical if one uses the $V(n_i - \frac{1}{2})(n_{i+1} - \frac{1}{2})$ form, which involves interactions between unoccupied sites.

### C. Experimental realizations

The most promising route toward observing and exploiting the reported phenomena arguably involves coupled optical-cavity arrays [4,7]. In the past few years, there has been

an active effort toward designing a range of lattice models based on coupled photon cavities, each doped with atoms. Neighboring cavities are coupled through intercavity photon tunneling, and the intracavity interplay between the atomic levels and photon modes determines the type of interaction. In particular, Ref. [4] has presented a scheme to realize an *XXZ* Hamiltonian, using atoms with a $V$-configuration level structure in resonance with the cavity. It may be expected that such a system can be realized in the laboratory within the time scale of a decade or so. A particular advantage of such a setup would be that each cavity can be individually driven by external lasers, thus implementing single-site addressing, which is essential for protocols like the quantum switch described in Sec. V.

Another possible implementation is through Josephson junction arrays, which in some arrangements (persistent-current qubits [8,9]) are well described by an *XXZ* Hamiltonian, as detailed in Ref. [2]. Such arrays could be prepared in nonequilibrium initial states and single-qubit addressing should be straightforward, and thus could also be ideal for exploration of the physics described here.

The more traditional realization of *XXZ* chains are bulk materials with chain structures. There are several compounds whose spin physics are reasonably well described by $\Delta > 1$ *XXZ* Hamiltonians, such as $CsCoCl_3$ and $TlCoCl_3$ with $\Delta \sim 7$ [10,11], and $BaCo_2V_2O_8$ with $\Delta \sim 2$ [12]. Unfortunately, single-site addressing is generally not feasible, and nonequilibrium states generally relax rapidly to the ground state in bulk materials. Nevertheless, it may still be possible to probe the physics presented in this article. With the spins polarized completely by a magnetic field above the saturation threshold, a localized excitation (through neutrons or laser pulse) could depolarize a few sites, moving the system to a magnetization sector where edge states can be relevant. By applying an excitation near one end of the material, one can watch for response at the other end, which would indicate whether the excited block is locked or propagating. The recent experiments described in Ref. [13] provide a promising step in the direction of laser excitation followed by transport, although the focus there was on heat transport.

Finally, there is the possibility of using optical lattices to realize spin Hamiltonians in general [3,14] and *XXZ* lattices in particular [3]. An advantage of such setups would be the optical tunability of spin couplings. Such a cold-atom realization would have additional complications of realizing a well-defined edge and accounting for harmonic traps. Both these issues could in principle be mollified through trap-shape manipulation; however, this is not a well-developed technology. It might therefore be interesting to calculate how well the interaction-induced edge-locking phenomena survive when the sharp edge is replaced by a smoother boundary.

### D. Open issues

This work raises several issues demanding further investigation. One expects nonequilibrium dynamical effects and possibly additional localization phenomena associated with the substructures of the lower bands (Fig. 3), which are yet to be explored. Depending on the experimental realization(s) that become available, the effects of terms beyond the *XXZ* Hamiltonian relevant for the particular realization need to be analyzed, and new control protocols can be designed for the site-addressing methods that are possible. Finally, because the *XXZ* model is Bethe ansatz solvable even with open boundary conditions [15], it remains an open problem to find out how the fractal subband structures in the high-energy spectrum are reflected in the Bethe ansatz root structure.

## ACKNOWLEDGMENTS

The author thanks J.-S. Caux, F. Essler, S. Flach, F. Heidrich-Meisner, A. M. Läuchli, G. Orso, and T. Vojta for helpful discussions.

[1] See, for example, S. Bose, Phys. Rev. Lett. **91**, 207901 (2003); Contemp. Phys. **48**, 13 (2007).
[2] A. Lyakhov and C. Bruder, New J. Phys. **7**, 181 (2005).
[3] L.-M. Duan, E. Demler, and M. D. Lukin, Phys. Rev. Lett. **91**, 090402 (2003).
[4] A. Kay and D. G. Angelakis, Europhys. Lett. **84**, 20001 (2008).
[5] V. Pouthier, Phys. Rev. B **76**, 224302 (2007).
[6] R. A. Pinto, M. Haque, and S. Flach, Phys. Rev. A **79**, 052118 (2009).
[7] M. J. Hartmann, F. G. S. L. Brandão, and M. B. Plenio, Nat. Phys. **2**, 849 (2006); A. D. Greentree, C. Tahan, J. H. Cole, and L. C. L. Hollenberg, *ibid.* **2**, 856 (2006); D. G. Angelakis, M. F. Santos, and S. Bose, Phys. Rev. A **76**, 031805(R) (2007); M. J. Hartmann, F. G. S. L. Brandão, and M. B. Plenio, Phys. Rev. Lett. **99**, 160501 (2007); D. Rossini and R. Fazio, *ibid.* **99**, 186401 (2007); M. Paternostro, G. S. Agarwal, and M. S. Kim, New J. Phys. **11**, 013059 (2009).
[8] L. S. Levitov, T. P. Orlando, J. B. Majer, and J. E. Mooij, e-print arXiv:cond-mat/0108266.
[9] J. E. Mooij, T. P. Orlando, L. Levitov, L. Tian, C. H. van der Wal, and S. Lloyd, Science **285**, 1036 (1999).
[10] H. Yoshizawa, K. Hirakawa, S. K. Satija, and G. Shirane, Phys. Rev. B **23**, 2298 (1981); J. P. Goff, D. A. Tennant, and S. E. Nagler, *ibid.* **52**, 15992 (1995).
[11] A. Oosawa, Y. Nishiwaki, T. Kato, and K. Kakurai, J. Phys. Soc. Jpn. **75**, 015002 (2006).
[12] S. Kimura, H. Yashiro, K. Okunishi, M. Hagiwara, Z. He, K. Kindo, T. Taniyama, and M. Itoh, Phys. Rev. Lett. **99**, 087602 (2007).
[13] M. Otter, V. V. Krasnikov, D. A. Fishman, M. S. Pshenichnikov, R. Saint-Martin, A. Revcolevschi, and P. H. M. van Loosdrecht, J. Magn. Magn. Mater. **321**, 796 (2009).
[14] J. J. Garcia-Ripoll, M. A. Martin-Delgado, and J. I. Cirac, Phys. Rev. Lett. **93**, 250405 (2004).
[15] F. C. Alcaraz, M. N. Barber, M. T. Batchelor, R. J. Baxter, and G. R. W. Quispel, J. Phys. A **20**, 6397 (1987).